A reassessment of SuperDARN meteor echoes from the upper mesosphere and lower thermosphere ☆

Gareth Chisham *, Mervyn P. Freeman

British Antarctic Survey, Natural Environment Research Council, High Cross, Madingley Road, Cambridge CB3 0ET, United Kingdom

ABSTRACT

The Super Dual Auroral Radar Network (SuperDARN) is a network of HF radars used to study phenomena in the Earth's magnetosphere, ionosphere, and upper atmosphere. Phenomena in the upper mesosphere and lower thermosphere (MLT) can be studied as the SuperDARN radars act effectively as meteor radars at near ranges. However, SuperDARN meteor echo measurements from all heights have typically been combined together to give a height-averaged picture of large-scale characteristics and dynamics of the MLT. This is in part due to the uncertainty in the measurement of individual meteor echo heights, which is in turn partly due to the lack of reliable (and for some radars, the lack of any) interferometric information. Here, we present a method for calibrating SuperDARN interferometer data which reduces the systematic offsets in meteor echo height estimations. Using 9 years of SuperDARN data we then determine occurrence distributions of SuperDARN meteor echo heights. The distributions are approximately Gaussian with height, extending from ~75 to ~125 km and peaking around ~102–103 km. In addition, we investigate whether the Doppler spectral width measured by the SuperDARN radars, which is related to the ambipolar diffusion coefficient for meteor echoes, can be used as a proxy measurement for meteor echo height. Due to the large spread of spectral width measurements at any one height we conclude that this proxy measurement is not practical and that the height of individual SuperDARN meteor echoes cannot be estimated without interferometric information. We also discuss how more accurate height information could be used to study the height variation of neutral wind velocities and the ambipolar diffusion coefficient across the MLT altitude range, and conclude that SuperDARN meteor echo observations have the potential to complement, and significantly extend the altitude range of, meteor echo observations from standard VHF meteor radars.

© 2013 The Authors. Published by Elsevier Ltd. All rights reserved.

1. Introduction

For over 30 years, meteor radars have proven to be important instruments for studying dynamical processes in the upper mesosphere and lower thermosphere (MLT) regions of the Earth's upper atmosphere. When meteoroids enter the Earth's atmosphere they ablate producing approximately cylindrical ionized meteor trails, with lifetimes ~0.01–10 s, that drift under the influence of winds in the neutral atmosphere. Radio waves can be backscattered from these meteor trails producing echoes that provide tracers of neutral atmospheric conditions and dynamics (e.g., McKinley, 1961; Ceplecha et al., 1998). Hall et al. (1997) first showed that the majority of radar echoes measured by the Super Dual Auroral

Radar Network (SuperDARN) at ranges less than 500 km are meteor echoes. This expanded the scientific potential of the SuperDARN radars to include the study of neutral atmosphere phenomena such as winds, planetary waves and tides in the MLT region (e.g., Jenkins et al., 1998; Jenkins and Jarvis, 1999; Bristow et al., 1999; Hussey et al., 2000; Espy et al., 2005; Malinga and Ruohoniemi, 2007; Hibbins et al., 2007, 2009, Hibbins et al., 2010a,b, 2011).

Two different types of meteor echo are identified by meteor radars (Thomas et al., 1988; Ceplecha et al., 1998): Overdense echoes occur where the electron density in the meteor trail is sufficiently large to totally reflect the transmitted radio wave. These echoes are very strong and can last several seconds, but are rare. Underdense echoes occur where the electron density in the meteor trail is lower and where the radio waves are scattered by individual free electrons in the trail. These represent the majority of observed meteor echoes, but generally last much less than a second.

The height distribution of underdense meteor echoes is controlled by a combination of effects, the most important of which is

---

* Corresponding author. Tel.: +44 1223221532.
 E-mail addresses: gchi@bas.ac.uk (G. Chisham), mpf@bas.ac.uk (M.P. Freeman).

the existence of the underdense meteor echo height ceiling, which sets a limit on the maximum detection height for underdense meteor echoes (Thomas et al., 1986, 1988; Ceplecha et al., 1998). The meteor echo height ceiling is predominantly a consequence of the ionized meteor trails having a finite radial extent. The initial meteor trail radius is approximately proportional to the inverse of the atmospheric density. If this initial radius is greater than, or of the order of, a quarter of the transmitted radio signal wavelength, then radio returns from different parts of the trail will destructively interfere and the echo will be attenuated. As the density decreases with increasing height, this initial trail radius increases and so the probability of echo attenuation increases. As a consequence, the meteor echo height ceiling is approximately logarithmically proportional to the probing radio signal wavelength, and hence depends on the operational frequency of the radar. In addition, the average meteor echo height (and hence the likely height of peak occurrence of observable meteor echoes) is also a function of frequency (Thomas et al., 1988), with that for lower frequencies in the HF range (3–30 MHz) peaking at a much higher altitude than that for frequencies typically used in the VHF range (30–50 MHz) (Thomas et al., 1986; Olsson-Steel and Elford, 1987; Steel and Elford, 1991).

Most meteor radars, and hence, most meteor echo observations presented in the literature, are from VHF (or high HF) radars that operate in the 20–50 MHz range, and the altitude range of these measurements is typically curtailed at ~100 km by the meteor echo height ceiling effect. Consequently, VHF radars only detect a fraction of the meteor trails that occur in the vertical space above any geographic location. However, modern dedicated VHF meteor radars can determine the height of an individual meteor to within 1 km (e.g., Hocking et al., 2001) which allows for an accurate determination of the variation of atmospheric measurements and processes within their altitude range. This height resolution is essential to resolve gravity waves, which can have km-scale vertical wavelengths, and to measure vertical profiles of quantities such as neutral wind velocity and temperature, which have scale heights of ~km (Fritts and Alexander, 2003).

Low HF radars have the capability to measure meteor echoes over a wider range of altitudes resulting in a greater number of meteor echo measurements. For example, the SuperDARN radars can operate between 8 and 20 MHz, corresponding to a meteor echo height up to ~120 km or higher. However, a major limitation of the SuperDARN meteor echo data to date has been the lack of reliable estimation of the height of the echoes, due to a combination of uncertainties in measurements of the echo range and the elevation angle of arrival of the backscattered HF signal. Although many SuperDARN radars are equipped with interferometers that provide the capability to estimate the elevation angle, the interferometer measurements have often been viewed as unreliable, typically due to difficulties in calibrating the phase differences measured between the main and interferometer antenna arrays (e.g., Hussey et al., 2000). In addition, some SuperDARN radars do not have any interferometric capability which means that the echo height for these radars must be estimated by other means.

An alternative height-determination method that has been proposed is to use a parameter measured by the SuperDARN radars that varies systematically with height in the MLT region, and which could consequently provide a proxy for the meteor echo height. One such candidate is the Doppler spectral width w, first suggested as a potential proxy by Hall et al. (1997), which, for an underdense meteor echo, is inversely proportional to the exponential decay time τ of the backscattered power or proportional to the related ambipolar diffusion coefficient D_a (McKinley, 1961). Both linear and higher-order models have been fitted to VHF meteor radar measurements of height against $\log(1/\tau)$ (e.g., Hocking et al., 1997; Hocking, 1999; Hocking et al., 2001), and against $\log(D_a)$ (Greenhow

and Neufeld, 1955; Thomas et al., 1988; Tsutsumi et al., 1994). However, there is a large amount of scatter in these measurements, especially in large data sets (Tsutsumi et al., 1994; Chilson et al., 1996; Cervera and Reid, 2000; MacDougall and Li, 2001; Galligan et al., 2004) and consequently least squares fits (e.g., Galligan et al., 2004; Thomas et al., 1988) seem inappropriate as the correlation is often poor. This large amount of scatter is not unexpected as D_a depends on temperature and pressure and thus any variations in these will enhance the spread in aggregated measurements made over long time intervals. Indeed, it has been suggested that the decay time does not show a systematic variation with height (Ballinger et al., 2008) and that any meteor echo within the 90–100 km height region could be associated with any of the measured values of D_a (Galligan et al., 2004). Thus, many studies now reject the possibility of height determination through the use of either τ or D_a as a proxy as these meteor echo height estimates are likely to show substantial variability on an individual meteor basis.

As a consequence of the uncertainties in height estimation, SuperDARN meteor echo analysis has typically been limited to deriving the horizontal neutral wind velocity field by fitting a model to all meteor wind observations, taken from all heights and radar look directions over a 1-h interval (Bristow et al., 1999), with the assumption that this provides the best approximation of the meridional and zonal neutral wind components at an altitude ~93–95 km (Hall et al., 1997; Hussey et al., 2000). This has proven suitable for studying tides and planetary waves (Espy et al., 2005; Hibbins et al., 2007, 2009, 2010a,b, 2011).

We are only aware of two SuperDARN studies of the MLT that presented the variations of measured quantities with height. Hussey et al. (2000) compared neutral winds measured by the Saskatoon SuperDARN radar, averaged over a 2-week interval in order to study tidal variations, with nearby MF radar observations, at a height resolution of 3 km from 82 to 97 km. They concluded that the SuperDARN height resolution was poor due to the poor range resolution and ultimately decided not to use the interferometry data but to produce a single-height meteor wind product assuming an average meteor echo height of 95 km. Tsutsumi et al. (2009) used frequency domain interferometry to improve the accuracy of the SuperDARN meteor echo height determinations and subsequently estimated neutral wind components in 4 km height bins (at a height resolution of 2 km), covering the height range 84–110 km, over a 4-day interval. However, the frequency domain interferometry technique is presently not a part of standard SuperDARN operations.

In summary, due to the potential of increasing the height range of meteor echo measurements of the upper atmosphere, meteor radars operating in the 2–20 MHz range (including the SuperDARN radars which operate predominantly in the 10–15 MHz range) have much to offer, but only if more reliable estimates of meteor echo heights can be achieved and the limitations of the measurements are fully understood. In this paper we reassess SuperDARN meteor echoes by addressing the following questions: (1) What is the occurrence distribution of the height of SuperDARN meteor echoes, and can we improve SuperDARN interferometric measurements? (2) Can Doppler spectral width be used as a proxy for meteor echo height? (3) Can SuperDARN meteor echoes measured using standard SuperDARN operations be used to estimate the height variation of quantities such as neutral wind velocity and the ambipolar diffusion coefficient (and by extension, temperature), in the MLT region?

2. Method

2.1. Instrumentation and measurements

SuperDARN (Greenwald et al., 1995; Chisham et al., 2007) is an international network of over-the-horizon HF radars used to study

the upper atmosphere, ionosphere, and magnetosphere. It was originally designed to measure the magnetosphere–ionosphere convection electric field by combining multiple line-of-sight measurements of the motion of ionospheric F-region electron density irregularities (Villain et al., 1985) but has subsequently been shown to be capable of studying a wide range of upper atmospheric phenomena. Each SuperDARN radar is an electronically-steerable, narrow-beam, phased-array radar that typically comprises a main array of 16 log-periodic antennae. The standard 16-beam scan used by most of the radars creates a field of view for each radar that typically extends ~52° in azimuth and from ~180 km to more than 3000 km in range, usually sampled in 45 km range gates. The radars are frequency agile and can operate over a wide range of HF frequencies (from 8 to 20 MHz) allowing adaptation to different propagation conditions and phenomena. The radars transmit a multi-pulse sequence and the returned echoes are sampled and processed to produce multi-lag complex autocorrelation functions (ACFs) which are averaged over 3–6 s, and from which power, line-of-sight Doppler velocity, and Doppler spectral width are the primary products that are determined.

SuperDARN meteor echoes, observed at ranges < ~500 km, were first termed 'Grainy Near-Range Echoes' (GNREs) by Hall et al. (1997) because of the speckled appearance of the backscatter power variation on a range-time-intensity plot. This speckled appearance results from a seemingly random variation of the echo intensity from one integration period to the next, and from one range to the next, which is itself a result of the sporadic occurrence, size, and location, of meteor trails. Fig. 1 presents 'typical' meteor echo measurements from one day of data (17th April 2001) from beam 3 of the Saskatoon SuperDARN radar, for range gates 2 and 4, centred on 225 km (blue) and 315 km (orange) respectively. The backscatter power variation in Fig. 1a illustrates the seemingly random variation in intensity discussed above, with no systematic pattern in the variations. The line-of-sight velocity values (Fig. 1b) are very well defined (low errors) but there is a high degree of fluctuation, between ± 50 m/s, illustrating the dynamic nature of the MLT region and/or a vertically-

structured MLT sampled at the randomly varying heights of meteor echoes. The Doppler spectral width variations (Fig. 1c) are generally low (< 40 m/s), although on occasion can be higher, with values above 100 m/s. The elevation angle measurements (Fig. 1d) for each range lie approximately in a band ~10° wide, with the lower range echoes (in blue) characterised by higher elevation angles than the higher range echoes (in orange) in order to access the same meteor echo height region.

For underdense meteor echoes the power of the backscattered signal decays exponentially with time as the radius of the ionized trail increases due to a combination of processes such as ambipolar diffusion, eddy diffusion, and electron–ion recombination (e.g., Thomas et al., 1988; Cervera and Reid, 2000; Hocking, 2004), with ambipolar diffusion being thought to be the dominant process. The variation of the backscattered power of an underdense meteor echo, $P(t)$, with time, t, can therefore be written as

$$P(t) = P(0) \exp\left(-\frac{t}{\tau}\right) \qquad (1)$$

where $P(0)$ is the power at time $t=0$ (the formation of the meteor trail), and τ is a constant that characterises the decay time of the trail. Furthermore, assuming ambipolar diffusion, measurement of the decay time of an underdense meteor echo provides an estimate of the ambipolar diffusion coefficient (D_a) in the meteor trail (McKinley, 1961) using

$$D_a = \frac{\lambda^2}{32\pi^2\tau} \qquad (2)$$

where λ is the wavelength of the transmitted signal. Such estimates of D_a have been used to study temperature variations in the MLT (Hocking et al., 1997; Hocking, 1999) through the relationship

$$D_a = K_0 \frac{T^2}{p} \qquad (3)$$

where T and p represent the atmospheric temperature and pressure, respectively, and K_0 is a constant that depends upon the ionic components of the meteor trail. This obviously relies on them being a suitable model for the atmospheric pressure variation with altitude in this region.

Unlike dedicated meteor radars, it is not generally possible to directly measure the exponential decay rate of SuperDARN meteor echoes without operating in a special high time resolution mode known as the raw time series (or TMS) mode (Yukimatu and Tsutsumi, 2002; Tsutsumi et al., 2009). At present, the SuperDARN radars do not run this mode routinely because of the associated significant increase in data volume and processing complexity. However, provided a single meteor echo dominates the backscattered signal within the radar integration time of ~3–6 s, the ACF determined from standard SuperDARN operations provides the decay time of the meteor echo. For an underdense meteor echo, the Doppler spectral width (w) measured by the SuperDARN radars is related to the meteor decay time through the relationship

$$w = \frac{\lambda}{4\pi\tau} \qquad (4)$$

(Hall et al., 1997). Combining (2) and (4) results in the following expression for D_a in terms of w:

$$D_a = \frac{\lambda w}{8\pi} \qquad (5)$$

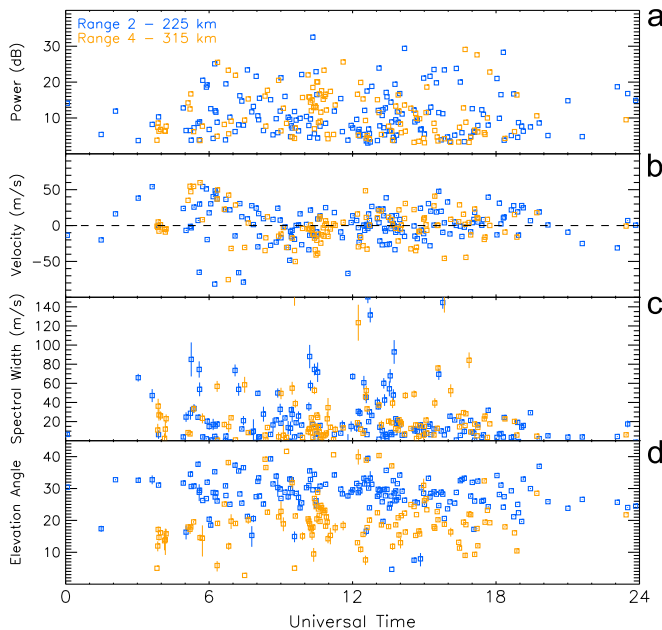allowing the estimation of the diffusion coefficient from SuperDARN meteor echo data.

Fig. 1. Example meteor echo data from one day of data (17th April 2001) from Saskatoon beam 3, and from range gates 2 (225 km—blue) and 4 (315 km—orange). The panels present the following quantities: (a) Backscatter power. (b) Line-of-sight Doppler velocity. (c) Doppler spectral width. (d) Elevation angle of arrival. (For interpretation of the references to colour in this figure caption, the reader is referred to the web version of this article.)

2.2. Signal propagation

It is important to understand for what ranges, and at what heights, we would expect SuperDARN meteor echoes to occur. We first consider the height range over which we would expect the SuperDARN radars to observe meteor echoes.

The upper limit on the observation height is a result of the underdense meteor echo height ceiling, as discussed in the introduction. The resultant echo power reduction, which increases with height, depends on: (1) The size of the initial meteor trail radius in comparison to the radar wavelength. This trail radius is dependent on the height and velocity of the meteor. (2) Diffusion during the formation of the meteor trail. This is dependent on the meteor velocity, the echo range, the radar wavelength, and the ambipolar diffusion coefficient D_a (McKinley, 1961; Thomas et al., 1988). In Fig. 2 we present examples of the variation of this echo power reduction with height for two HF (10 and 15 MHz) and two VHF (30 and 50 MHz) frequencies, using the expressions for the echo power reduction presented in Thomas et al. (1988). For these examples we use a typical meteor velocity of 40 km/s (Thomas et al., 1988) and an echo range of 270 km. The solid lines in Fig. 2 represent the echo power reduction determined using the model D_a variation with height presented in Thomas et al. (1988). However, the biggest uncertainty in these variations results from the wide range of values of D_a that are observed at any single height (e.g., Cervera and Reid, 2000). The dashed lines in Fig. 2 encompass the range of echo power reduction curves that can result given the typical range of observed values of D_a. Fig. 2 shows how the meteor echo height ceiling (where the echo power reduction reduces to zero) decreases in altitude with increasing frequency. The highest altitude at which one could expect to observe meteor echoes decreases from ~125 km for 10 MHz signals to ~105 km for 50 MHz. We can estimate from these results that the meteor echo height ceiling for SuperDARN meteor echoes at 10–15 MHz is in the range 108–125 km, depending on frequency and diffusion coefficient.

To estimate the lower limit on the observation height we make use of the observation that all studies generally report very low meteor echo counts below ~75–80 km for HF frequencies (Thomas et al., 1986; Hocking et al., 1997; Cervera and Reid, 2000; MacDougall and Li, 2001; Hocking et al., 2001).

The average meteor echo height for observations at a particular frequency can also be estimated. Using the relationship given by Thomas et al. (1988), the average meteor echo height for Super-DARN observations in the 10 to 15 MHz range should be ~104–107 km. However, this empirical relationship was based on an extrapolation from measurements made at VHF frequencies. Alternatively, examining the meteor echo height distributions presented by Thomas et al. (1986) and Olsson-Steel and Elford (1987), for which the distribution for 6 MHz operation peaked at 102 km and that for 25 MHz peaked at 98 km, we can estimate by interpolation that for the 10–15 MHz frequency range typically used by the SuperDARN radars the peak height of the meteor echo distribution should be at ~100 km.

In summary, we use the above reasoning to estimate that the meteor layer for SuperDARN radar observations at 10–15 MHz should extend over altitudes from ~ 75 to 125 km, peaking at a height ~100 km.

In Fig. 3 we present example SuperDARN HF propagation paths to this meteor layer in a realistic spherical geometry. Sample propagation paths for the first five ranges are illustrated by the solid coloured straight lines, representing range gates 1 (180 km—black line), 2 (225 km—blue), 3 (270 km—green), 4 (315 km—orange), and 5 (360 km—red). They are assumed to be straight-line propagation paths backscattering from the peak of the meteor layer (here taken as 100 km). Straight-line propagation
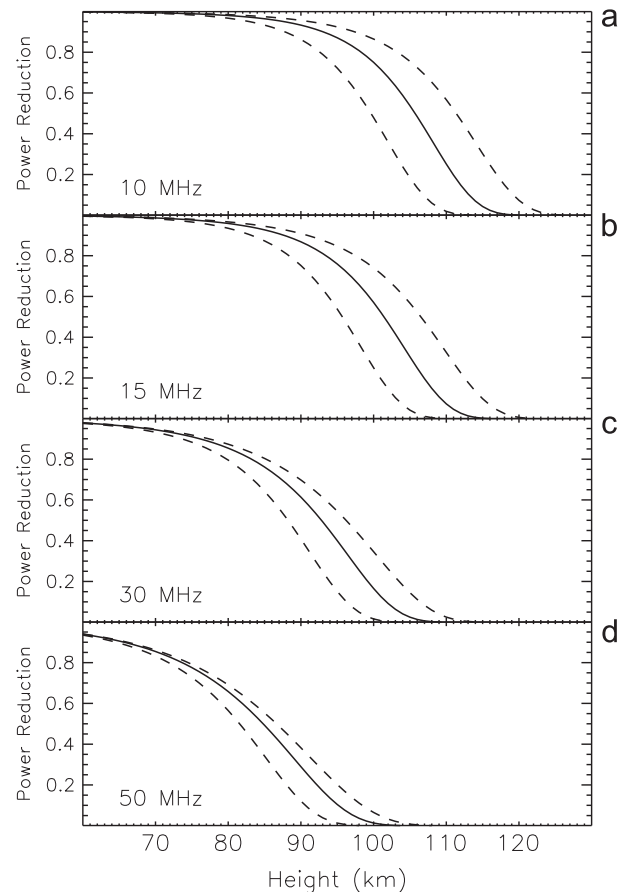

Fig. 2. Echo power reduction due to meteor echo height ceiling effects as a function of meteor echo height and radar frequency. The four panels present the variations for: (a) 10 MHz, (b) 15 MHz, (c) 30 MHz, and (d) 50 MHz. The solid lines represent the echo power reduction determined using the model ambipolar diffusion coefficient variation with height presented in Thomas et al. (1988). The dashed lines illustrate the range of echo power reduction curves that can result given the typical range of observed values of the diffusion coefficient.
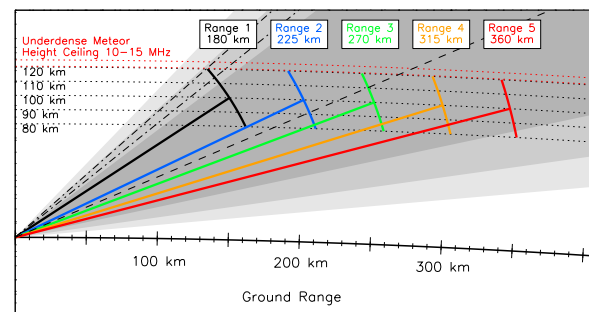

Fig. 3. Selected straight-line propagation paths (solid coloured lines) of signals reflected from the estimated centre of the meteor layer measured by the Super-DARN radars at 100 km. The coloured arcs at the ends of the lines indicate the angular region for each range that covers the bulk of the estimated meteor layer. The propagation paths are presented for the first five range gates: 1 (black), 2 (blue), 3 (green), 4 (orange), and 5 (red). The paths are presented in a realistic spherical geometry. Different heights within the meteor layer are indicated by black dotted lines. The maximum underdense meteor echo height ceiling for a 10–15 MHz signal is indicated by red dotted lines. The black diagonal dashed line highlights the takeoff angle of maximum gain in the vertical radiation pattern at 12 MHz. The grey shaded regions indicate the angular range within which the gain is within 3 dB (darkest shading), 6 dB, and 9 dB (lightest shading) of the maximum gain. The black diagonal dot-dashed lines highlight the maximum non-aliased elevation angles that can be measured by the SuperDARN radars at 12 MHz for the minimum and maximum beam azimuths (assuming a separation between the main and interferometer antenna array of 100 m). (For interpretation of the references to colour in this figure caption, the reader is referred to the web version of this article.)

is a fair assumption to this altitude as refraction is very weak below the E-region ionosphere (e.g., Villain et al., 1984). The coloured arcs at the ends of the propagation paths indicate the angular region for each range that covers the bulk of the meteor layer. Towards the top of this layer the assumption of straight-line propagation is likely to be less reliable at times due to the increasing electron density in the ionospheric E-region. The estimated maximum underdense meteor echo height ceiling (120–125 km) for the frequency range 10–15 MHz is indicated by the red dotted lines.

Although the actual distribution of meteors with height is typically the same whatever may the range of the measurement be, the amount of echoes measured will vary with range. A general reduction in measured echoes at all heights will occur with increasing range due to the dependence of power on range in the radar equation (see e.g., Thomas et al., 1988). In addition, some height dependent reductions in measured echoes will occur due to the angular variation of the antenna gain (see e.g., Arnold et al., 2001, 2003). The takeoff angle of the maximum gain in the SuperDARN vertical radiation pattern varies with frequency, being ~23° for 12 MHz (which is a typical frequency used). This is indicated by the diagonal dashed line in Fig. 3. Furthermore, for takeoff angles between ~12° and ~37° the signal is quite uniform, being the region where the gain is within 3 dB of its peak value. This is shown by the darkest grey shaded region in Fig. 3. The progressively lighter shaded regions show approximately the angular regions where the gain is within 6 dB, and 9 dB, of the maximum. Moving away from the angular region of peak gain into these regions will mean that weaker echoes from meteor trails will become progressively more difficult to detect as these are less likely to meet the minimum power threshold for measurement. As the range increases (e.g., toward the range 5 propagation path in red in Fig. 3) the takeoff angles of ray paths interacting with the meteor region move further away from the region of peak gain, and this effect is increased at lower altitudes where the ray paths are farthest from the region of peak gain, and hence, where the weaker echoes may go undetected. This may result in a bias of measured meteor echoes at the further ranges towards slightly higher altitudes when compared to those ranges for which the propagation paths to the complete range of potential meteor echo heights are close to the region of peak gain (e.g., ranges 2 and 3). A similar effect, but in the opposite sense, occurs at the nearest range (i.e., range 1) where there may be a bias towards echoes at lower altitudes, and some echoes at the highest altitudes in the meteor region may go undetected.

2.3. Interferometry

Many of the SuperDARN radars have interferometer arrays which enable estimation of the elevation angle of arrival of the returned signal (Milan et al., 1997; André et al., 1998), and hence the meteor echo height, provided the approximation of straight line propagation is a reasonable assumption. The receive-only interferometer array comprises typically four antennae located at some distance (~100–200 m) either in front of, or behind, the main array used for transmitting and receiving the HF signals. The measurement of phase differences in the returned signals between the main and interferometer arrays allows the determination of the elevation angles of arrival.

The elevation angle α of the backscattered signal measured by the SuperDARN radars is given by

$$\sin \alpha = \left(\cos^2 \phi_0 - \frac{\Psi_P^2}{|\mathbf{k}|^2 d^2} \right)^{1/2} \tag{6}$$

where d is the shortest distance between the main and interferometer arrays, i.e., along the radar boresight that lies perpendicular to both the main and interferometer antenna arrays, ϕ_0 is the beam azimuth angle, i.e., the angle between the beam direction and the radar boresight at an elevation angle of $\alpha = 0°$, $|\mathbf{k}|$ is the magnitude of the wavevector of the backscattered HF radio signal, and Ψ_P is the phase difference between the backscattered signals arriving at the main and interferometer arrays. This phase difference can also be written as

$$\Psi_P = |\mathbf{k}|\delta P \tag{7}$$

where δP is the path difference between the signals returning to the main and interferometer arrays.

The phase difference is measured by taking the zero lag phase in the cross-correlation function between the main and interferometer return signals. As a consequence of the wavelength of the signal being less than the path difference δP, the measured phase difference Ψ_0 ($-\pi \leq \Psi_0 < \pi$) is related to the actual phase difference along the path, Ψ_P, by

$$\Psi_P = \Psi_0 + 2n\pi - \delta\psi_c \tag{8}$$

where n is an integer that must be determined, and where $\delta\psi_c$ relates to that part of the measured phase difference that does not result from differences in the paths of the backscattered signals to the two antenna arrays. This additional phase difference is ideally zero and is often assumed as such in elevation angle calculations because it is generally difficult to estimate. It results from instrumental features such as differing cable lengths to the main and interferometer arrays and differences in the signal travel time in the radar electronics. $\delta\psi_c$ relates to an additional time delay in the system of δt_c given by

$$\delta\psi_c = |\mathbf{k}|c\delta t_c \tag{9}$$

where c is the speed of light.

The integer n in Eq. (8) is determined by assuming that the maximum phase difference that can be measured (Ψ_{max}) is that for $\alpha = 0°$ (when the path difference δP is the greatest), and that the true phase difference (Ψ_P) most likely lies between this maximum and the first 2π ambiguity, i.e.,

$$\Psi_{max} - 2\pi < \Psi_P \leq \Psi_{max} \tag{10}$$

Hence, Ψ_{max} is determined by setting $\alpha = 0°$ in Eq. (6) giving

$$\Psi_{max} = |\mathbf{k}|d \cos \phi_0 \tag{11}$$

Subsequently, n is adjusted so that Ψ_P is within the expected range given in Eq. (10). This assumption only remains valid if the true elevation angle is less than a maximum value α_{max} relating to the situation when $\Psi_P = \Psi_{max} - 2\pi$. If the true elevation angle is greater than α_{max} then aliasing occurs, giving an erroneous measurement. For 12 MHz operation and for $d = 100$ m (typical for SuperDARN interferometers), α_{max} varies between 38.7° and 41.4°, depending on the beam azimuth direction. These limits are shown by the black dot-dashed diagonal lines in Fig. 3. (For 10 MHz operation these limits range from 42.4° to 45.6°; for 15 MHz operation they range from 34.6° to 36.9°.) Hence, from inspection of Fig. 3, the upper end of the distribution of elevation angle measurements for range gate 1 will be affected by this cutoff, which will produce a maximum height cutoff for the range gate 1 height distribution. These aliased values will obviously then add to the number of erroneous height values elsewhere in the distribution, reducing the reliability of the distribution overall.

Assuming straight line propagation of the HF signal and a spherical Earth with average radius $R_E = 6371$ km, the height of the meteor echoes can be estimated using

$$h(r, \alpha) = (R_E^2 + r^2 + 2rR_E \sin \alpha)^{1/2} - R_E \tag{12}$$

(Chisham et al., 2008), where r is the range, and α is the elevation angle.

Uncertainty in this height estimate (σ_h) results from a combination of uncertainty in the exact range to the meteor trail (σ_r—a result of the standard SuperDARN 45 km range gate sampling) and uncertainty in the elevation angle estimation (σ_α—which can be estimated as part of the data processing). The height uncertainty is determined through the error equation

$$\sigma_h^2 = \frac{\sigma_r^2(r + R_E \sin \alpha)^2 + \sigma_\alpha^2(rR_E \cos \alpha)^2}{R_E^2 + r^2 + 2rR_E \sin \alpha} \tag{13}$$

Uncertainty in the range estimation can be reduced by either reducing the range gate sampling distance (e.g., to 15 km) or by using techniques such as frequency domain interferometry (e.g., Tsutsumi et al., 2009). However, neither of these are part of standard SuperDARN operations.

2.4. Data selection

We choose, in the first instance, to examine SuperDARN data from the Saskatoon radar (geographic co-ordinates: 52.16°N, 106.53°W), as there is evidence from previous studies that the Saskatoon interferometric data are relatively reliable (e.g., André et al., 1998; Chisham et al., 2008; Ponomarenko et al., 2009). In addition, we perform the same analysis on SuperDARN data from the Prince George radar (geographic co-ordinates: 53.98°N, 122.59°W) to check that the results are not radar specific. We use data from the time interval covering the years 1996–2004 inclusive (2000–2004 for Prince George) and combine data from a selection of beams (those numbered 3, 6, 9, 12), with different look directions, approximately 9.75° apart. We only use data from the first 5 range gates (180–360 km) where we expect the backscattered signals to be heavily dominated by meteor echoes. We restrict our observations to those made using frequencies in the range 10–15 MHz, for which contaminating backlobes and side-lobes in the antenna radiation pattern are reduced.

We use the SuperDARN data processing routine FitACF version 2 (Ponomarenko and Waters, 2006) to determine the standard SuperDARN products of backscatter power, line-of-sight Doppler velocity, and Doppler spectral width from the measured ACFs at each range and time. This is an improved version of the original SuperDARN FitACF algorithm (e.g., Villain et al., 1987; Baker et al., 1995). FitACF applies a linear least squares fit to the phase of the ACF as a function of lag to determine the Doppler velocity, and, assuming an exponential decorrelation of the ACF magnitude as a function of lag, applies a linear least squares fit to the logarithm of the magnitude of the ACF to determine the Doppler spectral width. In order to remove poor and noisy data we initially apply a minimum power threshold of 3 dB above the sky noise.

Although we expect most of the echoes measured in the first five ranges to be meteor echoes, there is still the possibility of contamination from other sources, e.g., auroral E-region echoes, sporadic-E echoes, and polar mesosphere summer echoes (PMSE). In addition, there may be instances where echoes from more than one meteor trail are identified at a particular range within an integration period, with the ACF resulting from the mixture of echoes likely to be interpreted erroneously. Hence, it is important to eliminate as many of these contaminating echoes as possible from our data set. Meteor echoes are typically characterised by extremely low velocity errors (typically < 1 m/s). E-region echoes and mixed echoes will generally have larger velocity errors. From a study of the velocity error of different types of backscatter in the first 12 range gates (180–720 km) (not shown) it can be seen that the E-region echoes are ~4 times more likely than meteor echoes to have a velocity error greater than 5 m/s. By further examining

the distribution of the velocity error of suspected meteor echoes in the first 5 range gates (not shown) we can see that the average velocity error of meteor echoes decreases exponentially with increasing backscatter power, the high power echoes being significantly better defined (e.g., for a power $> \sim 15$ dB the velocity error is typically < 1 m/s). From inspection of this distribution we choose a rejection threshold for the velocity error of meteor echoes that varies exponentially with power, starting at 10 m/s for 0 dB and reducing to 0.2 m/s for 50 dB. Similarly, by inspection of the distribution of spectral width error of possible meteor echoes in the first 5 range gates (not shown) we choose a rejection threshold for the spectral width error of meteor echoes that varies exponentially with power, starting at 40 m/s for 0 dB and reducing to 0.6 m/s for 50 dB.

3. Results

3.1. What is the occurrence distribution of the height of SuperDARN meteor echoes?

In Fig. 4a, we present occurrence distributions of the elevation angle of arrival from the Saskatoon SuperDARN radar for the five range gates of interest, using the same colour scheme to denote range as in Fig. 3. The distributions are approximately Gaussian in shape with the mode of the distributions decreasing with increasing range. This is expected given the geometry of the propagation paths for meteor echoes illustrated in Fig. 3. There is also a small background population spread over a wide range of elevation angles. At elevation angles less than the peak region, this background population most likely results from anomalous phase measurements introduced by aliasing. At elevation angles higher than the peak region, the background population may be a result of contamination by overdense meteor echoes and ionospheric E-region echoes.

Fig. 4b presents the associated occurrence distributions of echo height determined using Eq. (12). The mode of the distributions increases with range from ~100 km for range gate 1 to ~115 km for range gate 5. There is also an increase in the width of the
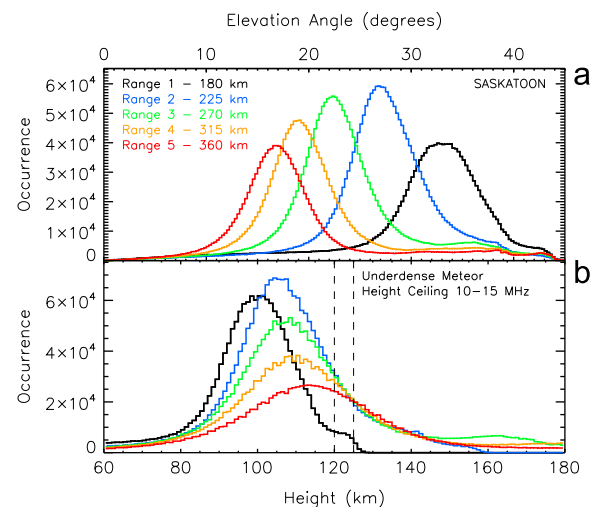

Fig. 4. (a) Occurrence distributions of elevation angles of arrival (0.5° bin size) as measured by Saskatoon beams 3, 6, 9, and 12 combined, during the years 1996–2004 inclusive. (b) Occurrence distributions of meteor echo height (1 km bin size) determined from the distributions of elevation angles of arrival in panel (a). The distributions in both panels are presented for the first five range gates: 1 (black), 2 (blue), 3 (green), 4 (orange), and 5 (red). The vertical dashed lines in panel (b) indicate the maximum altitude of the underdense meteor echo height ceiling for a 10–15 MHz signal. (For interpretation of the references to colour in this figure caption, the reader is referred to the web version of this article.)

height distributions with increasing range (the full width at half maximum varies from ~25 km for range gate 2 to ~35 km for range gate 5). We suggest that this latter observation is a result of an increase in random errors in the phase determinations and the greater contribution of uncertainties in the elevation angle in the more oblique propagation paths for the farther ranges, e.g., the mean uncertainty determined solely from the measured elevation angle uncertainties for range gate 1 height estimates is ~1.2 km, whereas that for range gate 5 height estimates is ~3.5 km, with a much larger variance. The vertical dashed lines in Fig. 4b indicate the maximum altitude of the underdense meteor echo height ceiling for ~10–15 MHz, above which we would expect very few meteor observations. In this figure, a significant number of meteor echo height estimations are located above this altitude, for the reasons given above.

The echo height distributions presented in Fig. 4b contain features that suggest that there may be a systematic error in the echo height determinations. This is because we observe deviations from the following expectations:

(1) The height range of the echo height distribution should be similar for all ranges, with the same peak height, if the echo source is the same distribution of meteors. We might expect to see an increase in the distribution spread with range (as is observed) because of increasing random errors for farther ranges, as discussed above. However, the peak height should be invariant. This assumes that there are no major variations due to the angular variation of the antenna gain and the elevation angle cutoff, as discussed in Sections 2.2 and 2.3. This might be an issue for ranges 1 and 5.
(2) There should be very few echoes from above the meteor echo height ceiling, except as a result of the spread of the distribution due to random errors, aliasing, overdense meteor echo contamination or ionospheric contamination.

If we make the assumption that the effect of HF refraction at these altitudes, and for these elevation angles, is typically small, as is suggested by ray trace modelling (e.g., Villain et al., 1984), then the unexpected systematic variation in the peak of the meteor echo height distribution is most likely a result of a calibration issue with the elevation angle data. We assume this to be due to the uncertainty surrounding the additional phase term $\delta\psi_c$ in Eq. (8). Following this assumption, it is possible to apply a correction to reduce this systematic error and to provide better echo height estimates. Consequently, we calibrate the meteor echo height estimates by assuming the following:

(1) That the main source of the systematic offsets in the height distributions is the uncertainty in the value of δt_c (and consequently in $\delta\psi_c$).
(2) That any errors introduced by refraction of the HF signal path at higher altitudes are less than or similar to the uncertainties in the measured quantities.
(3) That the meteor echo height distributions are approximately Gaussian and that the distributions for different ranges should peak at the same altitude.

Hence, we vary the value of δt_c (which is frequency independent, in contrast to $\delta\psi_c$), and select the value that best aligns the meteor echo height distributions for range gates 2, 3, and 4 (for which we expect the most similar distributions). We achieve this by finding the value of δt_c that minimises the squares of the differences between the modes of the distributions for ranges 2, 3, and 4. These modes are estimated by fitting a Gaussian with a background quadratic function to the height distributions. This analysis results in a value of $\delta t_c = -2.7$ ns for the Saskatoon data,

equivalent to a phase offset $\delta\psi_c \sim -0.065\pi$ for 12 MHz operation. In Fig. 5 we replot the data from Fig. 4, but here the elevation angle and meteor echo height distributions have been determined after inclusion of the additional phase offset. The three height distributions used in the calibration are now successfully co-aligned, with the average of the modes for range gates 2, 3, and 4 being 102.7 km (indicated by the vertical red dashed line in Fig. 5). This is very close to 100 km which was our predicted modal value based on previous studies, as discussed in Section 2.2. In addition, the height distributions for range gates 1 and 5 are also better aligned but biased to lower and higher altitudes, respectively, as expected given the discussion in Sections 2.2 and 2.3.

In order to illustrate the generality of this calibration method for other SuperDARN radars, we present, in Fig. 6, the result of the same analysis applied to meteor echo data from the Prince George SuperDARN radar. However, in this case, the calibration factor was estimated to be $\delta t_c = +2.6$ ns. The calibrated Prince George height distributions are very similar to those for Saskatoon (Fig. 5), with the average of the modes for range gates 2, 3, and 4, being 102.8 km for this radar (indicated by the red dashed line in Fig. 6), extremely close to the value for Saskatoon. One difference is the existence of a bias in the range gate 5 distribution towards higher altitudes, as discussed in Section 2.2, which was not as large in the Saskatoon data. This difference between the two radars may be a result of differences in the operational frequencies used by Prince George and Saskatoon, or because the Prince George measurements only cover the years 2000–2004. Reproducing the Saskatoon distributions for the subset of years 2000–2004 (not shown) introduces a larger bias in the range gate 5 distribution towards higher altitudes similar to the Prince George distribution, which lends support to this explanation.

The fact that a calibration factor with a different sign was required for the Prince George radar, and that the difference between the calibration factors for the two radars is ~5.3 ns, is further evidence that the observed systematic variations result from uncertainties in the phase calibration (which are likely to be
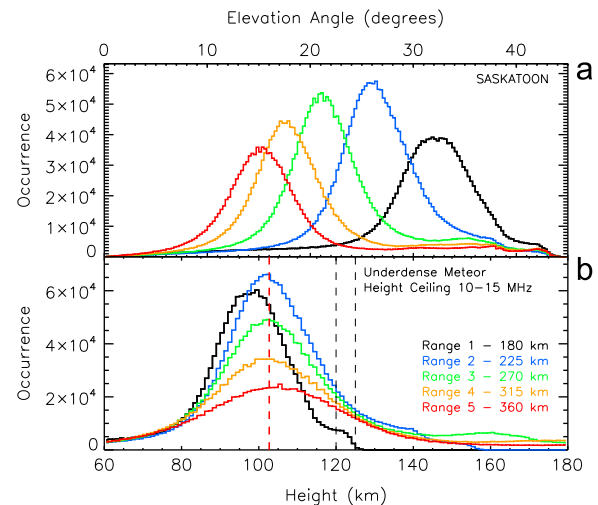

Fig. 5. (a) Occurrence distributions of calibrated elevation angles of arrival (0.5° bin size) as measured by Saskatoon beams 3, 6, 9, and 12 combined, during the years 1996–2004 inclusive (see text for details of calibration). (b) Occurrence distributions of calibrated meteor echo height (1 km bin size) determined from the distributions of calibrated elevation angles of arrival in panel (a). The distributions in both panels are presented for the first five range gates: 1 (black), 2 (blue), 3 (green), 4 (orange), and 5 (red). The black vertical dashed lines in panel (b) indicate the expected maximum altitude of the underdense meteor echo height ceiling for a 10–15 MHz signal. The red vertical dashed line highlights the average of the modes of the calibrated meteor echo height distributions for range gates 2, 3, and 4 at 102.7 km altitude. (For interpretation of the references to colour in this figure caption, the reader is referred to the web version of this article.)
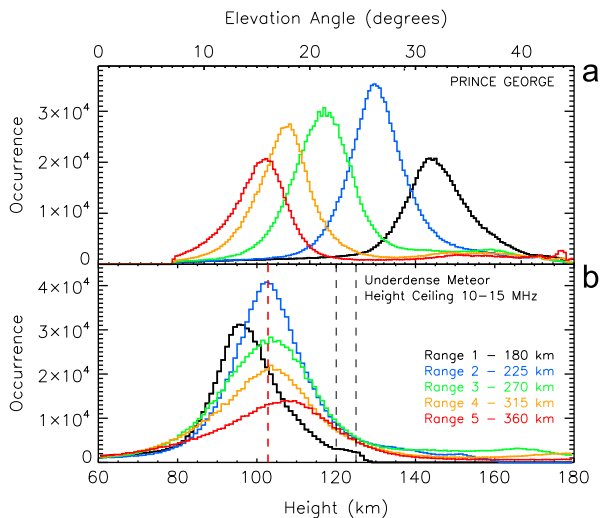
Fig. 6. (a) Occurrence distributions of calibrated elevation angles (0.5° bin size) of arrival as measured by Prince George beams 3, 6, 9, and 12 combined, during the years 2000–2004 inclusive (see text for details of calibration). (b) Occurrence distributions of calibrated meteor echo height (1 km bin size) determined from the distributions of calibrated elevation angles of arrival in panel (a). The distributions in both panels are presented for the first five range gates: 1 (black), 2 (blue), 3 (green), 4 (orange), and 5 (red). The black vertical dashed lines in panel (b) indicate the expected maximum altitude of the underdense meteor echo height ceiling for a 10–15 MHz signal. The red vertical dashed line highlights the average of the modes of the calibrated meteor echo height distributions for ranges 2, 3, and 4 at 102.8 km altitude. (For interpretation of the references to colour in this figure caption, the reader is referred to the web version of this article.)
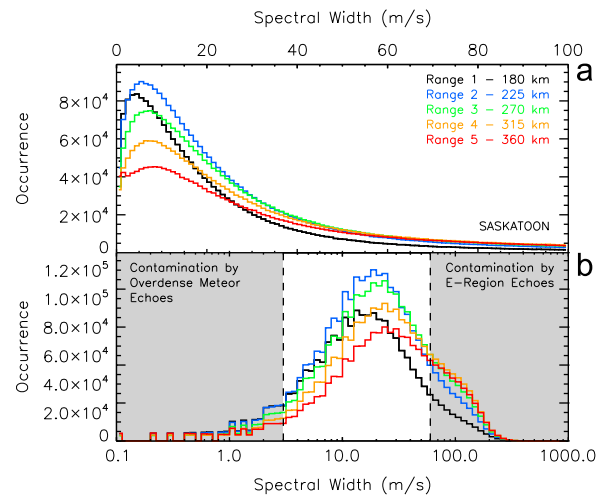

Fig. 7. Occurrence distributions of Doppler spectral width measured by Saskatoon beams 3, 6, 9, and 12 combined, during the years 1996–2004 inclusive. The distributions are presented for the first five range gates: 1 (black), 2 (blue), 3 (green), 4 (orange), and 5 (red). (a) The distributions plotted using a linear spectral width scale with linear binning (1 m/s bin size). (b) The distributions plotted using a logarithmic spectral width scale with logarithmic binning (0.05 bin size). The two grey-shaded regions indicate areas of the distributions that may be contaminated by non-underdense meteor echoes. (For interpretation of the references to colour in this figure caption, the reader is referred to the web version of this article.)

different for each radar), rather than from physical factors such as the effect of non-straight line propagation of the HF signal or of angular variation in the antenna gain (which are likely to be similar for every radar).

On the basis of these results, we conclude here that the height distribution of SuperDARN meteor echoes is approximately Gaussian with a maximum at ~102–103 km, and that it extends from ~75 to 125 km with a full width at half maximum of ~25–35 km.

3.2. Can Doppler spectral width be used as a proxy for meteor echo height?

The Doppler spectral width w measured routinely by the SuperDARN radars is related to the decay time τ of the meteor trail through Eq. (4), and hence, to the ambipolar diffusion coefficient, D_a, through Eq. (5) (see Section 2.1). As discussed above, it has previously been shown that both $\log(1/\tau)$ and $\log D_a$ show a systematic variation with height, with some studies promoting the existence of a linear relationship. Hence, a similar relationship between $\log w$ and height may be expected, and has been suggested (Hall et al., 1997; Jenkins et al., 1998). If an empirical relationship between spectral width and height could be determined then it would prove useful as a proxy measurement for the height of SuperDARN meteor echoes, especially for those SuperDARN radars without interferometer arrays. To investigate this possibility we study here the variation of the distribution of spectral width measurements with height in our data set.

We look first at the occurrence distributions of the Doppler spectral width of the meteor echoes, again using measurements from the first five ranges. These distributions are presented in Fig. 7a, for range gates 1–5 (using the same colour scheme to illustrate the range as in previous figures), using equally sized spectral width bins of 1 m/s. The distributions for each range all vary in a similar manner, peaking at a low value of spectral width (<10 m/s) with a long tail that extends to much higher values. The mode of this distribution increases with range from ~4 m/s for

range gate 1 (180 km) to ~8 m/s for range gate 5 (360 km). A similar variation was identified by Arnold et al. (2001) who showed that both the mode and the mean of the distribution of the Doppler spectral width of meteor echoes increased with range. Given the long-tailed nature of the observed spectral width distributions, and the fact that we might expect a relationship between $\log w$ and height, we replot the distributions in Fig. 7b using a log scale for the spectral width, and using equally sized bins of $\log w$. When plotted in this way the core of the spectral width distribution appears approximately Gaussian, with the mode of the distribution increasing slightly with range, as in Fig. 7a.

There are two regions within these distributions where there may be some contamination from backscattered signals that are not underdense meteor echoes, and these are highlighted by the grey shaded regions in Fig. 7b. Very low values of spectral width ($<~3$ m/s) are a characteristic of overdense meteor echoes (Hall et al., 1997; Jenkins et al., 1998). For overdense meteor echoes the relationship between spectral width and the meteor decay time (Eq. (4)) does not hold. Higher spectral width values ($>~60$ m/s) can be a characteristic of backscatter from ionospheric irregularities. Indeed, the distributions presented in Fig. 7b suggest the existence of contamination from such echoes in the form of a shoulder in the distribution around 100 m/s, especially for the farther ranges. Ionospheric echoes do not provide any information about the motion of the neutral atmosphere. Hence, we must use caution when interpreting measurements with these spectral width values.

In Fig. 8a we present the two-dimensional occurrence distribution of meteor echoes with height and Doppler spectral width, for the five ranges of interest. The red shaded regions represent the regions of highest occurrence and the blue, purple and white regions represent the regions of lowest occurrence. The data are presented as occurrence distributions rather than scatter plots due to the large number of samples involved (~10^6 for each range). The vertical black and white dotted lines highlight the spectral width values of 3 and 60 m/s, beyond which there is possible contamination by non-underdense meteor echoes. We restrict the distributions to measurements within the meteor layer (75–125 km).
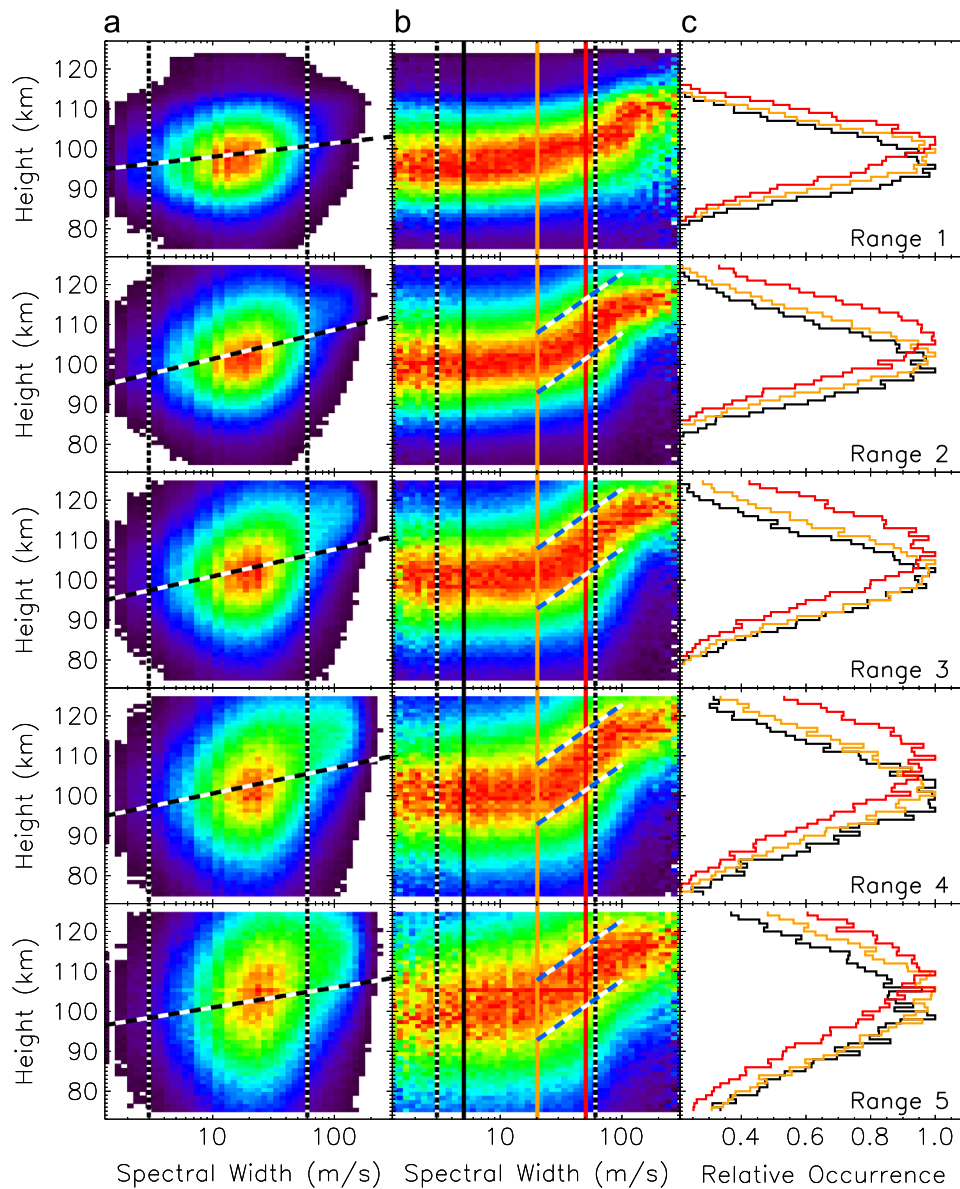
Fig. 8. (a) Two-dimensional occurrence distributions of meteor echoes with height and spectral width as measured by Saskatoon beams 3, 6, 9, and 12 combined, during the years 1996–2004 inclusive, and for range gates 1–5 (top to bottom). Colour scale ranges from red (high occurrence) to white (low occurrence). The black and white dashed lines represent Deming regression lines for the data set (see text for details). The black and white vertical dotted lines encompass the region within which the spectral width values should most reliably have a relationship with the meteor decay time, and hence the ambipolar diffusion coefficient, as highlighted in Fig. 7. (b) The same data set as in panel (a), but the data in each spectral width bin has been normalised to show more clearly the variation of the height profile with spectral width. The blue and white dashed lines illustrate the region where the distribution shows a linear variation of height with log w. The black, orange, and red vertical dotted lines indicate the spectral width values of 5, 20, and 50 m/s. (c) Cuts through the occurrence distribution as shown in column (b) for spectral width values of 5 m/s (black distribution), 20 m/s (orange distribution), and 50 m/s (red distribution). (For interpretation of the references to colour in this figure caption, the reader is referred to the web version of this article.)

The contours of the occurrence distributions are approximately elliptical in shape with signs of a trend of increasing spectral width with increasing height. Some previous studies have applied linear regressions to their data sets to quantify the linear trends in $\log(1/\tau)$ or $\log D_a$ with height. The Pearson product-moment correlation coefficient for our distributions ranges from ~0.11 to ~0.20 which implies that there is only a small linear correlation between $\log w$ and height. However, due to the large amount of samples in each distribution the p-value in each case is < 0.001, implying that the correlation is highly significant. However, basic linear regressions are inappropriate when applied to two sets of independently measured variables with independent measurement errors. Here, we apply Deming regression to the data, an 'errors-in-variables' model that takes into account the errors in the observations of both quantities (Deming, 1943). This method requires knowledge of the ratio of the

variances of the errors of the two variables. For our data set, this can be estimated from the data sources. The results of the Deming regression for each of the 5 range gates are shown in Fig. 8a by the black and white dashed lines. The regression lines for range gates 2–5 are very similar, and show clearly the trend of increasing spectral width with increasing height. However, they do not represent particularly good models for the variation of spectral width with height due to the large spread of measurements about the trend. Hence, models of this type are wholly unsuitable for estimating the height of individual meteors from measurements of spectral width.

The spread in the observed values is very large, much wider than most VHF radar meteor echo observations that have compared height with either $\log(1/\tau)$ or $\log D_a$, which were made at the lower end of our altitude range (~80–100 km) (e.g., Tsutsumi et al., 1994; Hocking et al., 1997, 2001; Galligan et al., 2004).

However, data sets that were compiled over extended time intervals (e.g., Cervera and Reid, 2000; MacDougall and Li, 2001) show a similar spread in measurements to our observations. As the spread in the distributions is likely due to variations in temperature, pressure, and the ionic species found in the meteor trails (through Eq. (3), e.g., Cervera and Reid, 2000), this spread will increase with the size of the data set used. Hence, our use of 9 years of data is consistent with the large spread of measurements that we observe.

The occurrence distributions, as presented in Fig. 8a, do not clearly convey the full information about the height distribution associated with specific spectral width values. As we are trying to evaluate whether individual spectral width values can be used as a proxy for height we choose to redisplay in Fig. 8b the occurrence data shown in Fig. 8a, but with the addition of normalising the distribution in each spectral width bin so that the variation of the distribution of height with spectral width is clearer. Again, the red shaded regions represent the regions of highest normalised occurrence, and the darkest blue and purple regions represent the regions of lowest normalised occurrence. In addition, in Fig. 8c we present three cuts through the distribution in Fig. 8b, at spectral width values of 5 m/s (black distribution), 20 m/s (orange distribution), and 50 m/s (red distribution), as highlighted by the black, orange, and red vertical lines in Fig. 8b.

The distributions in Fig. 8b are roughly similar for the five selected ranges and can be broadly described by splitting into two spectral width regions:

(1) $w < {\sim}20$ m/s: Here, the distribution of meteor echo heights appears to show little variation with spectral width, being approximately centred around 100 km with a similar spread to the distributions presented in Figs. 3 and 4. This is shown more clearly by the comparison of the black (5 m/s) and orange (20 m/s) distributions presented in Fig. 8c, where the peak height of the distribution only differs by $< {\sim}3$ km. This clearly illustrates that any individual spectral width measurement could potentially relate to any meteor echo height in this spectral width range, and as a result it is an unsuitable proxy measurement. It is not clear if there is any physical reason for this lack of variation. It may be that the relationship between the true meteor decay time and the spectral width (Eq. (4)) becomes less reliable for smaller spectral width values, as other factors may also be influencing the measured spectral width within the radar integration time.

(2) $w > {\sim}20$ m/s: Here, the distribution of meteor echo heights appears to show an approximately linear variation with log w, with the centre of the distribution increasing from ~100 km at $w{\sim}20$ m/s to ~115 km at $w{\sim}100$ m/s. This is the case for range gates 2–5 (range gate 1 shows a smaller increase). The blue and white dashed lines are schematic lines encompassing the peak occurrence region (in red) to highlight this approximately linear increase and its similarity from range to range (the lines are at the same locations in each panel). Although there is a clear relationship between the meteor echo height and log w in this spectral width region, the width of the distribution is still too large to be able to make an accurate estimate of the height of individual meteor echoes from the spectral width measurement. This is clear from the large overlap between the orange (20 m/s) and red (50 m/s) distributions in Fig. 8c. However, this observation suggests that the spectral width measurements may potentially be useful for statistical/climatic variations with height, at least between 20 and 60 m/s, corresponding to a range of ~100 to ~110 km.

When the Saskatoon data set is reduced to month-sized intervals (not shown), the spread of the distributions is slightly reduced, but not significantly enough to show a clearer relationship between height and spectral width. We conclude from this that there is still significant variability in the diffusion coefficient (due to fluctuations in temperature, etc.) on these smaller time-scales that precludes a useful relationship between spectral width and height.

Analysis of the data for the Prince George radar (not shown) shows very similar results to Saskatoon. One difference is that the approximately linear region between ~20 and ~100 m/s is not so well defined.

We conclude here that, although there is a significant trend of increasing log w with height, SuperDARN measurements of Doppler spectral width (w) cannot practically be used as a proxy for the height of individual meteor echoes, consistent with similar suggestions that measurements of τ and D_a made by other individual meteor radars are also unsuitable as meteor echo height proxies. Consequently, interferometric information is crucial for determining the height of individual meteor echoes.

3.3. Can SuperDARN meteor echoes be used to estimate the height variation of measured quantities in the MLT?

The ability to accurately estimate the height of individual meteor echoes significantly increases the potential of the other measured quantities to study processes in the MLT region. Here, we assess whether individual meteor echo measurements from standard SuperDARN operations, which are routinely available at higher spatial and temporal resolution than the 1-h averaged SuperDARN measurements typically used in the past, can be used to determine height profiles of quantities such as velocity or diffusion coefficient across the MLT. This involves assessing the level of uncertainty in these measurements.

In Fig. 9 we present an example of individual Saskatoon SuperDARN meteor echo measurements of horizontal velocity and diffusion coefficient with height, measured by a near-meridional beam (beam 3) covering the time interval 1000–1100 UT on 16th April 2002. The horizontal velocity measurements have been determined from the line-of-sight velocity measurements by assuming that the vertical neutral wind velocity is negligible and by using the measured elevation angle and meteor echo height. The diffusion coefficients have been estimated from the Doppler spectral width measurements using Eq. (5). The height uncertainties have been estimated using Eq. (13), the velocity uncertainties have been estimated from the line-of-sight velocity error, and the diffusion coefficient uncertainties have been estimated from the measured spectral width error. Each individual point is colour-coded by range, using the same convention as in the previous figures. The vertical dotted line (and grey shaded region) in Fig. 9a indicates the 1-h averaged meridional wind velocity (and uncertainty) measured for this interval using the method of averaging typically used in SuperDARN MLT studies (e.g., Bristow et al., 1999).

Looking first at Fig. 9a, there is a wide range of measured velocity values from the individual meteor echoes (from ~−60 to ~50 m/s) but most of the measured values are clustered around the '1-h averaged' value (~−20 m/s). There appears to be no obvious systematic variation of the velocity with height or with range. Although these measurements do not show an obvious height variation of velocity for this hour, they do illustrate the level of fluctuations that exist in this time period. Looking next at Fig. 9b, there is a slight suggestion that the estimated diffusion coefficient is increasing with height but this is far from conclusive. Again there is a wide range of measured values (from ~1 to ~100 m^2/s), providing an estimate of the level of fluctuations in the data set. From browsing through a greater number of intervals we have assessed that the character of these intervals is not atypical. Hence, although Fig. 9 shows little evidence of systematic
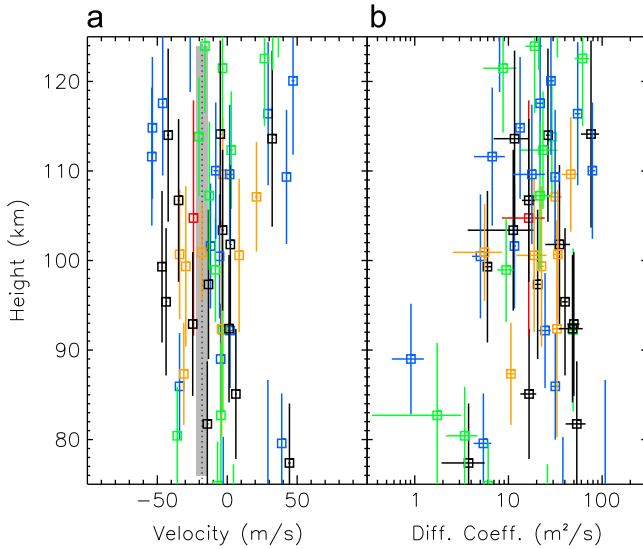
Fig. 9. Individual meteor echo measurements of (a) the meridional wind velocity, and (b) the ambipolar diffusion coefficient determined from measurements of Doppler spectral width using Eq. (5), covering an hour of Saskatoon beam 3 data from 1000 to 1100 UT on 16th April 2002. The values in both panels are determined for the first five range gates: 1 (black), 2 (blue), 3 (green), 4 (orange), and 5 (red). The vertical dotted line and grey shaded region represent the average meridional wind value and uncertainty, respectively, estimated for this hour using the standard SuperDARN method. (For interpretation of the references to colour in this figure caption, the reader is referred to the web version of this article.)

variations with height or range, it provides some idea of the level of fluctuations in the velocity and the diffusion coefficient.

Here, we use a statistical approach to extend this assessment to the wider data set. As illustrated in Fig. 9a, the uncertainty in the meteor echo line-of-sight velocity estimates is typically very small (with error bars often smaller than the vertical line width) as the measurements are generally very precise (i.e., the ACF phase variation is highly linear). However, the large amount of variability from one velocity measurement to the next has led people in the past to question the accuracy of the velocity measurements. The precise nature of the velocity measurements shows that this variability is not due to measurement uncertainty but represents actual small-scale velocity fluctuations due to gravity waves and turbulence.

In Fig. 10, we present the cumulative distribution function of the ratio between the uncertainty of individual meteor echo velocity measurements and the standard deviation of the corresponding hourly velocity data for the whole Saskatoon data set. This figure confirms that this ratio is generally very low, with ~97% of measurements having a ratio < 0.1 and ~40% of measurements having a ratio < 0.01. Thus the individual meteor echo velocity error is much less than the level of velocity fluctuation. Hence, the SuperDARN meteor echo data contain much more information about the level of fluctuation in the neutral wind velocity than has previously been made use of. This may prove useful in studying gravity wave activity and turbulence in the MLT region (e.g., using methods similar to Mitchell and Beldon, 2009). However, this level of variability, and the random nature of the location and occurrence of the meteor trails, is likely to make snapshot height profiles of velocity difficult to determine. However, it should be possible to study the height variation of quantities such as the velocity variance which would provide information about the vertical variation of dynamic processes in the MLT.

In contrast to the small uncertainties in the velocity measurements in Fig. 9a, the uncertainties in height are relatively large. The red occurrence distributions in Fig. 11 represent the
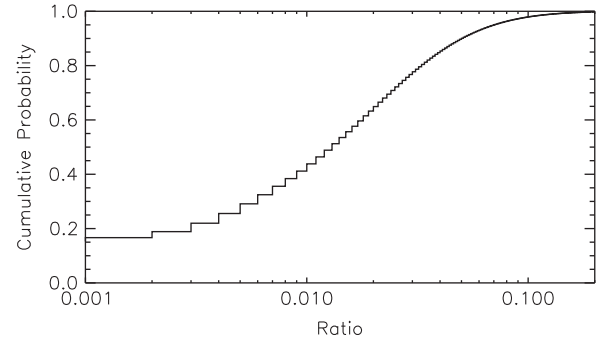

Fig. 10. The cumulative distribution function of the ratio between the uncertainty of individual meteor echo velocity measurements measured by Saskatoon beam 3 and the standard deviation of the corresponding hourly velocity data.
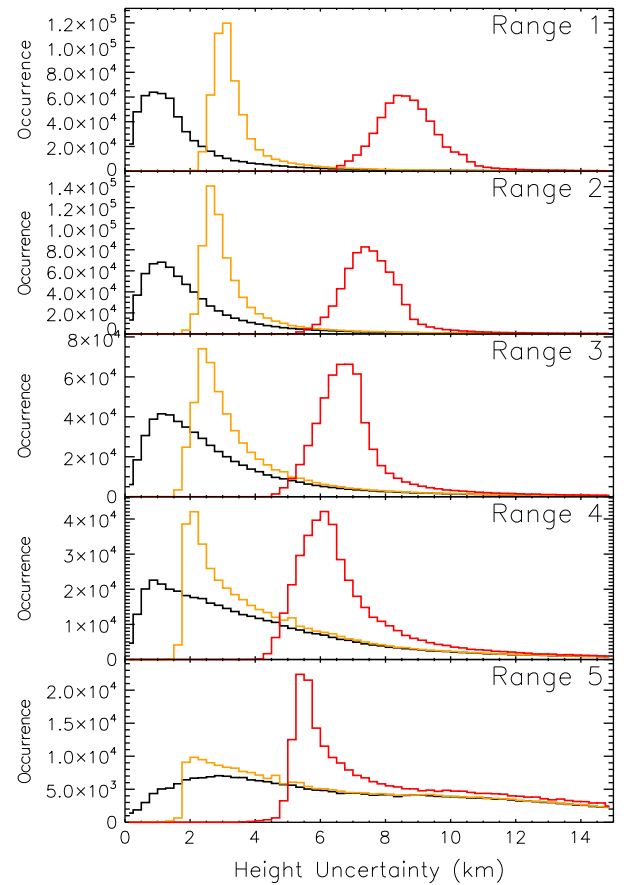

Fig. 11. Occurrence distributions of the height uncertainty from Saskatoon beam 3, range gates 1–5, covering the interval 1996–2004. The red distributions represent the true distributions for this data set with a range uncertainty based on 45 km range gates. The orange distributions represent the predicted distributions that would result using 15 km range gates. The black distributions represent the predicted distributions if the range uncertainty was negligible (e.g., if frequency domain interferometry was being used), and are a result of elevation angle uncertainties only. (For interpretation of the references to colour in this figure caption, the reader is referred to the web version of this article.)

distributions of the height uncertainties (determined using Eq. (13)) for the whole Saskatoon data set, and show the variation of the distribution with increasing range. These measurements assume 45 km range gate sampling. The mode of the distribution is largest at the lower ranges (~8.5 km for range gate 1). This is a result of the increasing contribution of the range uncertainty to the height uncertainty for greater elevation angles. This modal value decreases with increasing range (to ~5.5 km for range gate

5), but the mean and variance of the distribution increase due to the increasing contribution of the elevation angle uncertainty to the height uncertainty for more oblique propagation paths. This level of height uncertainty is a limitation, and most likely precludes the accurate measurement of the height variation of phenomena with small vertical wavelengths.

Hence, we conclude here that there is a potential for using SuperDARN meteor echo measurements in the MLT to study the level of fluctuations in the measured quantities that has so far been underexploited, but the uncertainty in the height measurements limits the scope of the measurements that can be made. Further intercomparisons of standard 45 km range measurements with higher resolution measurements (as in Tsutsumi et al., 2009) are needed to fully assess the accuracy of the height determinations made using standard SuperDARN operations.

4. Discussion

4.1. Regarding the measured height distribution

In Section 3.1 we concluded that the height distribution of SuperDARN meteor echoes is approximately Gaussian with a maximum at 102–103 km, and that it extends from ~ 75 to 125 km. Consequently, the ability of the SuperDARN radars to measure meteor echoes over this extended height range opens up possibilities for observations of neutral wind measurements in the lower thermosphere that are not open to VHF meteor radars that are typically restricted to ~80–100 km.

However, there is a discrepancy between our measurements of the height of maximum occurrence of SuperDARN meteor echoes and earlier estimations of the average SuperDARN meteor echo height by Hall et al. (1997) and Hibbins and Jarvis (2008). Hall et al. (1997) compared meteor echo measurements from the Saskatoon SuperDARN radar with co-located MF radar measurements from different altitudes (primarily comparisons of the phase of the semi-diurnal tide) to conclude that the average SuperDARN meteor echo height was 94 ± 3 km. Similarly, Hibbins and Jarvis (2008) compared meteor echo measurements from the Halley SuperDARN radar with co-located observations from an Imaging Doppler Interferometer (IDI) covering a range of altitudes and concluded that the winds and tides observed by the SuperDARN radar correlated best with those measured by the IDI in the height range 90–95 km. Ever since the observations of Hall et al. (1997), subsequent SuperDARN meteor echo studies (e.g., Hussey et al., 2000; Malinga and Ruohoniemi, 2007; Hibbins et al., 2007; Hibbins and Jarvis, 2008; Hibbins et al., 2009, 2010a, 2011) have assumed a value in the range 90–95 km as the average SuperDARN meteor echo height, and hence, as the best estimate for the height of the observations.

The reason for the discrepancy between our present results and these earlier observations is presently unclear. One possibility is that our measured meteor echo heights are being over-estimated as a consequence of our assumption of straight line propagation paths. We would argue against this based on the comparison between the Saskatoon and Prince George meteor echo height data sets. Before the measured meteor echo height distributions for these two radars are calibrated, the height distributions measured by the two radars are significantly different, with the distributions from one radar characterised by an increase in peak meteor height with range (Saskatoon) and the other showing a decrease in peak height with range (Prince George). Once the calibration factors are included for both radars, the peak meteor heights line up for most ranges (range gates 2–5), and for both radars. If the assumption of straight line propagation was an issue then we would expect it to affect the height distributions

measured by the two radars in a similar fashion. We do not see this. Alternatively, there is the possibility that the average Super-DARN meteor echo heights determined by Hall et al. (1997) and Hibbins and Jarvis (2008) have been underestimated. This could have occurred as a consequence of the large-scale averaging of SuperDARN meteor echoes from a wide range of altitudes to determine the amplitude and phase of the tidal signatures at the peak meteor echo height location. Alternatively, it could have resulted from the data selection criteria used in these studies, such as excluding echoes characterised by a spectral width greater than 25 m/s. Further work is needed to resolve this discrepancy.

Only one other study has presented a full probability distribution of SuperDARN meteor echo height similar to those presented in this paper. Tsutsumi et al. (2009) presented a distribution of meteor echo heights measured by the Cutlass Finland SuperDARN radar that peaked at ~95–96 km and extended from ~70 to 120 km. However, they did not separate their observations by range in the same manner as we have, and so a detailed comparison is difficult. On initial observation their results would appear to match previous conclusions about the average height of SuperDARN meteor echoes, as discussed above. However, Tsutsumi et al. (2009) did not appear to consider the effect that the elevation angle cutoff, discussed in Section 2.3, would have on their measured height distributions. The Cutlass Finland radar has a separation between the main and interferometer antenna arrays of 180 m. For 11 MHz operation (as used by Tsutsumi et al., 2009), the elevation angle cutoff ranges from ~30.1° to ~32.0°, depending on beam direction. This significantly biases their meteor echo measurements to lower altitudes, especially for range gate 2, which has the highest proportion of meteor echoes. Hence, the overall height distributions of Tsutsumi et al. (2009) are very likely to be affected in a similar way to our range gate 1 height distribution which peaked at a lower altitude due to this effect. Those meteor echoes with higher elevation angles will be aliased and so for much of the higher altitude meteor echo population their true height will not be estimated. For SuperDARN radars with a 100 m antenna array separation (such as Saskatoon and Prince George) this should only be a problem for range gate 1 meteor echoes.

If our conclusion that the peak height of SuperDARN meteor echoes is ~102–103 km is correct, then this would require a reassessment of earlier SuperDARN meteor echo studies, and should be considered in future SuperDARN meteor echo studies that use averaged data sets. Assuming a higher average meteor echo height of 102.5 km has a very small effect on horizontal wind estimates previously determined assuming a height of 95 km, reducing them by ~3% (for range gate 1) to ~1% (for range gate 5). However, better estimates of the most-likely echo height are more important when considering the interpretation of measurements, as processes vary significantly over small height ranges in the MLT region. In addition, the height assumption affects the comparison of SuperDARN meteor echo observations with measurements from other instruments for which more accurate estimates of height can be made.

4.2. Regarding the accuracy of individual meteor echo height determinations

It is clear that more accurate height measurements would increase the value of SuperDARN meteor echo measurements. Two ways of reducing the uncertainty of individual SuperDARN meteor echo height measurements would be (i) using 15 km range gates, and (ii) using frequency domain interferometry (Tsutsumi et al., 2009). Both these methods would reduce the range uncertainty that contributes to the height uncertainty. However, both methods are not yet part of standard SuperDARN operations.

In Fig. 11 we present predictions of the improvements that these methods would make to reducing the height uncertainty. The orange occurrence distributions in Fig. 11 represent the predicted distributions of height uncertainty in the case of 15 km range gate operation, assuming the same uncertainties in the elevation angle as in the measured (45 km range gate) red occurrence distributions, but with a reduced range uncertainty. The mode of these distributions ranges from ~ 2 to 3 km, however, the variance increases significantly with increasing range. The black occurrence distributions in Fig. 11 represent the predicted distributions of height uncertainty if frequency domain interferometry is being used, assuming the same uncertainties in the elevation angle as the measured uncertainty distributions, but with no uncertainty in range. The mode of these distributions is reduced to ~1 km for ranges 1–4, but again with larger variance at the further ranges.

This analysis shows that these techniques have the potential to significantly reduce the uncertainty in SuperDARN meteor echo height estimations, at least for ranges less than ~400 km.

4.3. Regarding measurements of the diffusion coefficient and temperature

There are uncertainties regarding the values of the diffusion coefficient determined from the Doppler spectral width, namely regarding the assumptions that the measured spectral width is due solely to the meteor echo decay, and that this in turn is controlled solely by the effects of ambipolar diffusion. A full assessment of these assumptions requires coincident meteor echo observations using both standard SuperDARN analysis and higher temporal resolution measurements of the meteor echo decay (e.g., Tsutsumi et al., 2009). There is also the potential for increased use of the high-resolution TMS mode for more routine measurement of meteor decay times in the future as the ability to record more data increases. This would provide improved estimates of the diffusion coefficient and improve the effectiveness of SuperDARN as a meteor radar network.

These improvements would be significant as one of the most useful height profiles that SuperDARN meteor echoes could provide would be temperature. Height profiles of temperature have been determined using meteor echo data from VHF meteor radars by exploiting the relationship with the ambipolar diffusion coefficient, as shown in (3) (Hocking et al., 1997; Hocking, 1999). This analysis clearly relies on having accurate and reliable measurements of the diffusion coefficient as well as a suitable model for the pressure variation across the MLT region.

4.4. Regarding electric and magnetic field effects on meteor trails above ~95 km

As the atmospheric density decreases with increasing altitude the collision frequency decreases significantly. This increases the influence of magnetic and electric fields on the meteor trails, resulting in anisotropic diffusion (Jones, 1991; Ceplecha et al., 1998; Robson, 2001). Below ~95 km the diffusion is isotropic but above ~95 km the Earth's magnetic field has an increasing effect on the shape of meteor trails as anisotropic diffusion leads to the formation of meteor trails with elliptical rather than circular cross-sections. Hence, the trail lifetime measured by a meteor radar depends on the angle at which the trail is seen by the radar relative to the magnetic field (Cervera and Reid, 2000). This leads to increasingly more scatter in measured decay times and diffusion coefficient measurements with increasing height. Although some

theoretical studies propose that at ~120 km the diffusion coefficient can vary by up to a factor of 100, depending on look direction (Jones, 1991; Cervera and Reid, 2000), there is no clear evidence for this effect, and it has been proposed that the effect is much smaller than the theory suggests (Elford and Elford, 2001; Galligan et al., 2004) with alternative processes acting at heights > 95 km which counteract the expected anisotropic diffusion effect. One such process is anomalous diffusion, as discussed by Dyrud et al. (2001). They suggested that up to ~105 km altitude the meteor trails expand at similar rates both along and across the magnetic field direction, due to the effect of anomalous diffusion. Hence, meteor trails remain more circular in cross-section than expected by previous theory, as has been observed by Galligan et al. (2004).

This uncertainty in the level of anisotropy in the meteor trails above ~95 km has a big effect on assessing the reliability of diffusion coefficient determinations (and consequently temperature variations) at these heights. For VHF radars, where the echoes come from lower than 100 km, these effects on the meteor trails are less important. For HF radars, such as the SuperDARN radars, observing at higher altitudes, it may be necessary to consider these effects. Hence, a better understanding of the diffusion processes is needed in order for the diffusion coefficient measurements to be viewed as wholly reliable. However, the SuperDARN velocity measurements will not be affected by these issues and can be reliably made across the whole MLT height range.

4.4.1. Regarding the interferometer phase calibration

As discussed in Section 2.3 and assessed in Section 3.1, any systematic offsets in the phase measurements made by the Super-DARN main and interferometer antenna arrays need to be determined in order that the measurements are properly calibrated and the meteor echo heights are as accurate as possible. In this paper, we have used a large amount of data from a long period of time to statistically determine a best estimate for this systematic offset. In reality, it is possible that this offset may change with time, varying slightly from one year to the next. It is also possible that it will change at times when the radar instrumentation and electronics are upgraded. There is also a possibility that the effect is frequency dependent. Any errors in the measurement of this offset will increase the error in the meteor echo height estimate. Subdividing the data set would allow the determination of the offset for smaller time epochs and frequency ranges resulting in measurements of the temporal variation of the offsets. This could lead to more accurate meteor echo height estimates.

5. Conclusions and summary

In the introduction of this paper we posed three questions regarding the analysis of SuperDARN meteor echoes. We conclude here by summarising our answers to these questions:

(1) The height distribution of SuperDARN meteor echoes is approximately Gaussian with a maximum of 102–103 km, and extends from ~ 75 to 125 km, with a full width at half maximum of ~ 25–35 km. The SuperDARN interferometric measurements can be improved by calibration of the interferometer data.

(2) Although there is a trend of increasing Doppler spectral width w with height, the spread around this trend means that SuperDARN measurements of w cannot practically be used as a proxy for the height of individual meteor echoes. Consequently, accurate interferometric information is crucial for determining the height of individual meteor echoes.

(3) There is potential for using standard resolution SuperDARN meteor echo data (better than 1-h averaging) that has so far

been underexploited. These data provide a measurement of the level of fluctuation of quantities such as velocity, and how this level of fluctuation varies with height. However, further inter-comparisons with special higher resolution measurements are needed to fully assess the accuracy of some of the measurements (e.g., height, diffusion coefficient) made using standard SuperDARN operations.

Acknowledgements

References

André, D., Sofko, G.J., Baker, K., MacDougall, J., 1998. SuperDARN interferometry: meteor echoes and electron densities from groundscatter. Journal of Geophysical Research 103, 7003–7015.

Arnold, N.F., Robinson, T.R., Lester, M., Byrne, P.B., Chapman, P.J., 2001. Super Dual Auroral Radar Network observations of fluctuations in the spectral distribution of near range meteor echoes in the upper mesosphere and lower thermosphere. Annales Geophysicae 19, 425–434.

Arnold, N.F., Cook, P.A., Robinson, T.R., Lester, M., Chapman, P.J., Mitchell, N., 2003. Comparison of D-region Doppler drift winds measured by the SuperDARN Finland HF radar over an annual cycle using the Kiruna VHF meteor radar. Annales Geophysicae 21, 2073–2082.

Baker, K.B., Dudeney, J.R., Greenwald, R.A., Pinnock, M., Newell, P.T., Rodger, A.S., Mattin, N., Meng, C.-I., 1995. HF radar signatures of the cusp and low-latitude boundary layer. Journal of Geophysical Research 100, 7671–7695.

Ballinger, A.P., Chilson, P.B., Palmer, R.D., Mitchell, N.J., 2008. On the validity of the ambipolar diffusion assumption in the polar mesopause region. Annales Geophysicae 26, 3439–3443.

Bristow, W.A., Yee, J.-H., Zhu, X., Greenwald, R.A., 1999. Simultaneous observations of the July 1996 2-day wave event using the Super Dual Auroral Radar Network and the High Resolution Doppler Imager. Journal of Geophysical Research 104, 12,715–12,721.

Ceplecha, Z., Borovicka, J., Elford, W.G., Revelle, P.O., Hawkes, R.L., Porubcan, V., Simek, M., 1998. Meteor phenomena and bodies. Space Science Reviews 84, 327–471.

Cervera, M.A., Reid, I.M., 2000. Comparison of atmospheric parameters derived from meteor observations with CIRA. Radio Science 35, 833–843.

Chilson, P.B., Czechowsky, P., Schmidt, G., 1996. A comparison of ambipolar diffusion coefficients in meteor trains using VHF radar and UV lidar. Geophysical Research Letters 23, 2745–2748.

Chisham, G., Lester, M., Milan, S.E., Freeman, M.P., Bristow, W.A., Grocott, A., McWilliams, K.A., Ruohoniemi, J.M., Yeoman, T.K., Dyson, P.L., Greenwald, R.A., Kikuchi, T., Pinnock, M., Rash, J.P.S., Sato, N., Sofko, G.J., Villain, J.-P., Walker, A.D.M., 2007. A decade of the Super Dual Auroral Radar Network (SuperDARN): Scientific achievements, new techniques and future directions. Surveys in Geophysics 28, 33–109.

Chisham, G., Yeoman, T.K., Sofko, G.J., 2008. Mapping ionospheric backscatter measured by the SuperDARN HF radars—Part 1: a new empirical virtual height model. Annales Geophysicae 26, 823–841.

Deming, W.E., 1943. Statistical Adjustment of Data. Wiley, New York.

Dyrud, L.P., Oppenheim, M.M., vom Endt, A.F., 2001. The anomalous diffusion of meteor trails. Geophysical Research Letters 28, 2775–2778.

Elford, W.G., Elford, M.T., 2001. The effective diffusion coefficient of meteor trails above 100 km (ESA 5.4). In: Proceedings of the Meteoroids 2001 Conference, Swedish Institute of Space Physics, Kiruna, Sweden.

Espy, P.J., Hibbins, R.E., Riggin, D.M., Fritts, D.C., 2005. Mesospheric planetary waves over Antarctica during 2002. Geophysical Research Letters 32, L21804, http://dx.doi.org/10.1029/2005GL023886.

Fritts, D.C., Alexander, M.J., 2003. Gravity wave dynamics and effects in the middle atmosphere. Reviews of Geophysics 41, 1003, http://dx.doi.org/10.1029/2001RG000106.

Galligan, D.P., Thomas, G.E., Baggaley, W.J., 2004. On the relationship between meteor height and ambipolar diffusion. Journal of Atmospheric and Solar-Terrestrial Physics 66, 899–906.

Greenhow, J.S., Neufeld, E.L., 1955. The diffusion of ionized meteor trails in the upper atmosphere. Journal of Atmospheric and Terrestrial Physics 6, 133–140.

Greenwald, R.A., Baker, K.B., Dudeney, J.R., Pinnock, M., Jones, T.B., Thomas, E.C., Villain, J.-P., Cerisier, J.-C., Senior, C., Hanuise, C., Hunsucker, R.D., Sofko, G., Koehler, J., Nielsen, E., Pellinen, R., Walker, A.D.M., Sato, N., Yamagishi, H., 1995. DARN/SuperDARN: a global view of the dynamics of high-latitude convection. Space Science Reviews 71, 761–796.

Hall, G.E., MacDougall, J.W., Moorcroft, J.-P., Manson, A.H., Meek, C.E., 1997. Super dual auroral radar network observations of meteor echoes. Journal of Geophysical Research 102, 14,603–14,614.

Hibbins, R.E., Espy, P.J., Jarvis, M.J., 2007. Quasi-biennial modulation of the semidiurnal tide in the upper mesosphere above Halley, Antarctica. Geophysical Research Letters 34, L21804, http://dx.doi.org/10.1029/2007GL031282.

Hibbins, R.E., Jarvis, M.J., 2008. A long-term comparison of wind and tide measurements in the upper mesosphere recorded with an imaging Doppler interferometer and SuperDARN radar at Halley, Antarctica. Atmospheric Chemistry and Physics 8, 1367–1376.

Hibbins, R.E., Jarvis, M.J., Ford, E.A.K., 2009. Quasi-biennial oscillation influence on long-period planetary waves in the Antarctic upper mesosphere. Journal of Geophysical Research 114, D09109, http://dx.doi.org/10.1029/2008JD011174.

Hibbins, R.E., Marsh, O.J., McDonald, A.J., Jarvis, M.J., 2010a. Interannual variability of the $S = 1$ and $S = 2$ components of the semidiurnal tide in the Antarctic MLT. Journal of Atmospheric and Solar-Terrestrial Physics 72, 794–800.

Hibbins, R.E., Marsh, O.J., McDonald, A.J., Jarvis, M.J., 2010b. A new perspective on the longitudinal variability of the semidiurnal tide. Geophysical Research Letters 37, L14804, http://dx.doi.org/10.1029/2010GL044015.

Hibbins, R.E., Freeman, M.P., Milan, S.E., Ruohoniemi, J.M., 2011. Winds and tides in the mid-latitude southern hemisphere upper mesosphere recorded with the Falkland Islands SuperDARN radar. Annales Geophysicae 29, 1985–1996.

Hocking, W.K., Thayaparan, T., Jones, J., 1997. Meteor decay times and their use in determining a diagnostic mesospheric temperature-pressure parameter: methodology and one year of data. Geophysical Research Letters 24, 2977–2980.

Hocking, W.K., 1999. Temperatures using radar-meteor decay times. Geophysical Research Letters 26, 3297–3300.

Hocking, W.K., Fuller, B., Vandepeer, B., 2001. Real-time determination of meteor-related parameters utilizing modern digital technology. Journal of Atmospheric and Solar-Terrestrial Physics 63, 155–169.

Hocking, W.K., 2004. Radar decay rate variability and atmospheric consequences. Annales Geophysicae 22, 3805–3814.

Hussey, G.C., Meek, C.E., André, D., Manson, A.H., Sofko, G.J., Hall, C.M., 2000. A comparison of Northern Hemisphere winds using SuperDARN meteor trail and MF radar wind measurements. Journal of Geophysical Research 105, 18,053–18,066.

Jenkins, B., Jarvis, M.J., Forbes, D.M., 1998. Mesospheric wind velocities derived from Super Dual Auroral Radar Network (SuperDARN) HF radar meteor echoes at Halley, Antarctica: preliminary results. Radio Science 33, 957–965.

Jenkins, B., Jarvis, M.J., 1999. Mesospheric winds derived from SuperDARN HF radar meteor echoes at Halley, Antarctica. Earth Planets Space 51, 685–689.

Jones, W., 1991. Theory of diffusion of meteor trains in the geomagnetic field. Planetary Space Science 39, 1283–1288.

MacDougall, J.W., Li, X., 2001. Meteor observations with a modern digital ionosonde. Journal of Atmospheric and Solar-Terrestrial Physics 63, 135–141.

Malinga, S.B., Ruohoniemi, J.M., 2007. The quasi-two day wave studied using the Northern Hemisphere SuperDARN HF radars. Annales Geophysicae 25, 1767–1778.

McKinley, D.W.R., 1961. Meteor Science and Engineering. McGraw Hill, New York.

Milan, S.E., Jones, T.B., Robinson, T.R., Thomas, E.C., Yeoman, T.K., 1997. Interferometric evidence for the observation of ground backscatter originating behind the CUTLASS coherent HF radars. Annales Geophysicae 15, 29–39.

Mitchell, N.J., Beldon, C.L., 2009. Gravity waves in the mesopause region observed by meteor radar: 1. A simple measurement technique. Journal of Atmospheric and Terrestrial Physics 71, 866–874.

Olsson-Steel, D., Elford, W.G., 1987. The height distribution of radio meteors: observations at 2 MHz. Journal of Atmospheric and Terrestrial Physics 49, 243–258.

Ponomarenko, P.V., Waters, C.L., 2006. Spectral width of SuperDARN echoes: measurement, use and physical interpretation. Annales Geophysicae 24, 115–128.

Ponomarenko, P.V., St-Maurice, J.-P., Waters, C.L., Gilles, R.G., Koustov, A.V., 2009. Refractive index effects on the scatter volume location and Doppler velocity estimates of ionospheric HF backscatter echoes. Annals of Geophysics 27, 4207–4219.

Robson, R.E., 2001. Dispersion of meteor trails in the geomagnetic field. Physical Review E 63, 026404.

Steel, D.I., Elford, W.G., 1991. The height distribution of radio meteors: comparison of observations at different frequencies on the basis of standard echo theory. Journal of Atmospheric and Terrestrial Physics 5, 409–417.

Thomas, R.M., Whitham, P.S., Elford, W.G., 1986. Frequency dependence of radar meteor echo rates. Proceedings of Astronomical Society of Australia 6, 303–306.

Thomas, R.M., Whitham, P.S., Elford, W.G., 1988. Response of high frequency radar to meteor backscatter. Journal of Atmospheric and Terrestrial Physics 50, 703–724.

Tsutsumi, M., Tsuda, T., Nakamura, T., Fukao, S., 1994. Temperature fluctuations near the mesopause inferred from meteor observations with the middle and upper atmosphere radar. Radio Science 29, 599–610.

Tsutsumi, M., Yukimatu, A.S., Holdsworth, D.A., Lester, M., 2009. Advanced Super-DARN meteor wind observations based on raw time series analysis technique. Radio Science 44, RS2006, http://dx.doi.org/10.1029/2008RS003994.

Villain, J.-P., Greenwald, R.A., Vickrey, J.F., 1984. HF ray tracing at high latitudes using measured meridional electron density distributions. Radio Science 19, 359–374.

Villain, J.-P., Caudal, G., Hanuise, C., 1985. A SAFARI-EISCAT comparison between the velocity of F-region small-scale irregularities and the ion drift. Journal of Geophysical Research 90, 8433–8443.

Villain, J.P., Greenwald, R.A., Baker, K.B., Ruohoniemi, J.M., 1987. HF radar observations of E region plasma irregularities produced by oblique electron streaming. Journal of Geophysical Research 92, 12,327–12,342.

Yukimatu, A.S., Tsutsumi, M., 2002. A new SuperDARN meteor wind measurement: raw time series analysis method and its application to mesopause region dynamics. Geophysical Research Letters 29, 1981, http://dx.doi.org/10.1029/2002GL015210.